

A few pA/$\sqrt{\text{Hz}}$ current sensor based on magnetoelectric effect

Yang Qiu(邱阳), Chengxuan Hu(胡成轩), Xiayu Zhou(周夏宇), Nanqi Zhou(周楠琦), Guoliang Yu(郁国良), Mingmin Zhu(朱明敏), Yan Li(李燕), Jiawei Wang(王嘉维), Aijun Song(宋爱军), Yanqi Wu(吴燕琪), Haomiao Zhou(周浩淼)

Citation: Chin. Phys. B. 35, 097502 (2026). DOI: 10.1088/1674-1056/ae1cb7 | CSTR: 32038.14.CPB.ae1cb7
http://cpb.iphy.ac.cn; http://iopscience.iop.org/cpb

What follows is a list of articles you may be interested in

Magnetic proximity-induced magnetoresistance in $Pt/Tm_3Fe_5O_{12}$ heterostructures

Zhengguo Liang(梁正国), Kunjie Dai(戴坤杰), Qiming Lv(吕崎鸣), Ao Wang(王傲), Jinfeng Zhang(章金凤), Lingfei Wang(王凌飞)

Chin. Phys. B. 35, 077512 (2026). DOI: 10.1088/1674-1056/ae5788 | CSTR: 32038.14.CPB.ae5788

Design of magnetoelectric coupling in ferroelectric metal

Wang Zhang(张旺), Xue-Zeng Lu(逯学曾)

Chin. Phys. B. 35, 077506 (2026). DOI: 10.1088/1674-1056/ae6173 | CSTR: 32038.14.CPB.ae6173

Oscillation of Dzyaloshinskii–Moriya interaction driven by weak electric fields

Runze Chen(陈润泽), Anni Cao(曹安妮), Xinran Wang(王馨苒), Yang Liu(柳洋), Hongxin Yang(杨洪新), Weisheng Zhao(赵巍胜)

Chin. Phys. B. 33, 027501 (2024). DOI: 10.1088/1674-1056/ad0f85

Insights into the regulation mechanism of ring-shaped magnetoelectric energy harvesters via mechanical and magnetic conditions

Yang Shi(师阳), Ni Li(李妮), Yong Yang(杨勇)

Chin. Phys. B. 30, 107503 (2021). DOI: 10.1088/1674-1056/abeee9

Equivalent circuit model including magnetic and thermo sources for the thermo–magneto–electric coupling effect in magnetoelectric laminates

Cui Xiao-Le(崔晓乐), Zhou Hao-Miao(周浩淼)

Chin. Phys. B. 24, 077506 (2015). DOI: 10.1088/1674-1056/24/7/077506

A few pA/$\sqrt{\text{Hz}}$ current sensor based on magnetoelectric effect

Yang Qiu(邱阳)[1], Chengxuan Hu(胡成轩)[1], Xiayu Zhou(周夏宇)[1], Nanqi Zhou(周楠琦)[1], Guoliang Yu(郁国良)[1], Mingmin Zhu(朱明敏)[1], Yan Li(李燕)[1], Jiawei Wang(王嘉维)[1], Aijun Song(宋爱军)[1], Yanqi Wu(吴燕琪)[2], and Haomiao Zhou(周浩淼)[1,†]

[1] *College of Information Engineering, China Jiliang University, Hangzhou* 310018, *China*
[2] *College of Metrology, Testing, and Instrumentation, China Jiliang University, Hangzhou* 310018, *China*

(Received 16 September 2025; revised manuscript received 30 October 2025; accepted manuscript online 7 November 2025)

Weak current sensors play a vital role in nuclear physics, quantum metrology, cryophysics, biomedicine, atmospheric measurement, and the semiconductor industry. In this paper, a weak current sensor based on the magnetoelectric (ME) effect is developed, consisting of a current–magnetic field conversion coil and an ME sensor composed of an ME sensing unit and a low-noise preamplifier. The equivalent magnetic field noise of the ME sensor at the resonant frequency of 15.96 kHz is 44.8 fT/$\sqrt{\text{Hz}}$, and the conversion coefficient is improved by optimizing the current–magnetic field conversion coil to suppress the equivalent current noise introduced by the ME sensor and the external environment. The weak current sensor has excellent linearity and current sensitivity, and the equivalent current noise at the resonant frequency reaches 8.4 pA/$\sqrt{\text{Hz}}$, which is 4 orders of magnitude lower than that of conventional ME current sensors.

Keywords: magnetoelectric (ME) effect, weak-current detection, weak current sensors

PACS: 75.85.+t, 77.55.Nv, 84.37.+q

DOI: 10.1088/1674-1056/ae1cb7 **CSTR:** 32038.14.CPB.ae1cb7

1. Introduction

The detection of weak current at the pico-ampere or even femto-ampere level is a critical enabling technology for frontier scientific research and advanced engineering applications.[1] For instance, scanning tunneling microscopy relies on precise measurement of weak tunneling current to achieve atomic-scale resolution imaging.[2] In quantum device research, accurate detection of current generated by single-electron transistors or quantum dot systems is essential for investigating quantum tunneling phenomena.[3] Furthermore, in experiments involving dark matter and neutrino detection, isolating faint fA-level signals from rare particle interactions necessitates ultra-sensitive current measurement techniques.[4] However, current detection presents severe challenges, including extremely low signal-to-noise ratio and complex environmental interference.[5] The accuracy of signal extraction and processing capabilities directly determines the resolution and reliability of advanced instrumentation.

Weak current sensors based on current–magnetic field conversion coils and weak magnetic field sensors exhibit advantages of low power consumption and low noise.[6] Among existing technologies, the superconducting quantum interference device (SQUID) achieves an equivalent magnetic field noise (EMN) of 0.15 fT/$\sqrt{\text{Hz}}$, making it one of the most sensitive magnetic field sensors available.[7] As the preferred solution for detecting weak current from transition-edge sensors, SQUID current sensors have found widespread application in astronomical detection, particle physics, and radiation measurement.[8–10] Antonio Vettoliere *et al*. reported a SQUID current sensor with double-washer schemes in either parallel or series, achieving an equivalent current noise (ECN) as low as 1 pA/$\sqrt{\text{Hz}}$–2 pA/$\sqrt{\text{Hz}}$.[11] Zhi Ni *et al*. developed and fabricated an LTS SQUID gradiometer using direct writing lithography technology, achieving an ECN of approximately 0.6 pA/$\sqrt{\text{Hz}}$.[12] Ethan Kleinbaum *et al*. proposed a 0.5-pA/$\sqrt{\text{Hz}}$ SQUID current sensor and further reduced the ECN to 2.3 fA/$\sqrt{\text{Hz}}$ using a superconducting coreless transformer with a gain of 212.[13] However, SQUID current sensors necessitate operation under ultra-low temperature conditions, while the requisite cryogenic refrigeration apparatus exhibits substantial volumetric constraints and prohibitive cost implications.[14] Although weak current sensors based on Hall sensors,[15] magnetoresistive sensors,[16] and fluxgates[17] have shown important application value in their respective application ranges, their ECN is relatively high, which cannot compare with SQUID current sensors.

The magnetoelectric (ME) sensors exhibit an optimal EMN of 3 fT/$\sqrt{\text{Hz}}$ at resonant frequency, rendering them exceptionally well-suited for weak current detection.[18] Dong *et al.* fabricated a compact quasi-ring type ME current sensor, demonstrating the EMN and ECN of 6 pT/$\sqrt{\text{Hz}}$ and 94 nA/$\sqrt{\text{Hz}}$ at the resonant frequency;[19] Yu *et al.* described the design and the implementation of a new structure for an AC current sensor based on an ME laminated composite slice, achieving the ECN of 15 mA/$\sqrt{\text{Hz}}$.[20] Zhang and Or devel-

†Corresponding author. E-mail: zhouhm@cjlu.edu.cn

© 2026 Chinese Physical Society and IOP Publishing Ltd. All rights, including for text and data mining, AI training, and similar technologies, are reserved.

oped a novel gradient-configuration ME current sensor employing paired magnetoelectric composite materials, which has the ECN of 0.6 μA/$\sqrt{\text{Hz}}$–14.3 mA/$\sqrt{\text{Hz}}$ in the frequency range of 1 Hz–170 kHz.[21] Although the EMN of ME sensors at resonant frequencies closely approaches that of SQUID, the ECN of ME current sensors fabricated using this principle remains significantly higher than that of SQUID current sensors. Obviously, given the application prospects of ultra-sensitive ME current sensors, theoretical research on noise suppression has become increasingly urgent.

In this work, a weak ME current sensor is proposed, encompassing a current–magnetic field conversion coil and an ME sensor consisting of an ME sensing unit and a low-noise preamplifier. Based on the mechanism of current–magnetic field–voltage conversion, corresponding signal and noise models are established to analyze the mechanism of noise generation and develop noise suppression methods for weak current detection. Afterwards, the low-noise current–magnetic field conversion coils are prepared, and their current noise introduced by the internal resistance is calculated. The magnetic field signal is then converted into an electrical signal using an ME sensing unit and a low-noise preamplifier. The results show that the weak current sensors based on the ME effect can achieve the ECN of 8.4 pA/$\sqrt{\text{Hz}}$ at the resonant frequency, which is 4 orders of magnitude lower than that of the traditional ME current sensor.

2. Implementation of the ME current sensor

The ME current sensor encompasses a current–magnetic field conversion coil and an ME sensor composed of an ME sensing unit and a low-noise preamplifier, as shown in Fig. 1. The finite-length solenoid Coil_{in}, as a current–magnetic field conversion coil, can convert the measured current signal I_{test} flowing through it into a magnetic field signal, with an internal resistance R and an inductance L. The ME sensing unit was placed at the central position inside the solenoid coil to convert magnetic field signals into electrical signals. Since this electrical signal is extremely weak, it needs to be further amplified by a low-noise preamplifier.

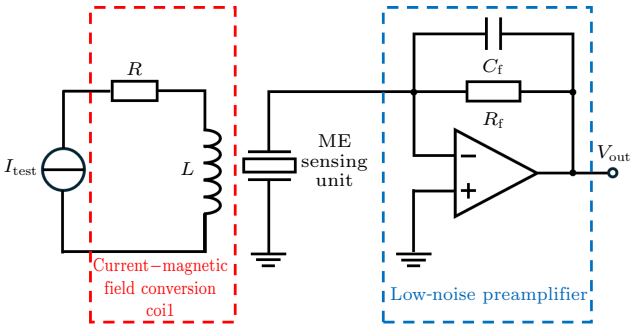


Fig. 1. Schematic diagram of weak current sensor based on ME effect.

The solenoidal coils are fabricated by tightly winding 0.5-mm diameter copper enameled wire onto cylindrical polycarbonate frames (inner diameter: 50 mm, outer diameter: 60 mm, length: 200 mm). Four prepared solenoidal coils (Coil I–Coil IV) feature a layer number (m) of 2, with lengths (l) of 5 mm, 25 mm, 100 mm, and 200 mm, and the number of turns (n) of each layer of the coil is 10, 50, 200, and 400, respectively, and its substance is shown in Fig. 2.



Fig. 2. The solenoid coils (Coils I–IV) with turns of 10, 50, 200, and 400 are tightly wound with copper enameled wire of 0.5 mm in diameter on the coil frame with an outer diameter of 60 mm.

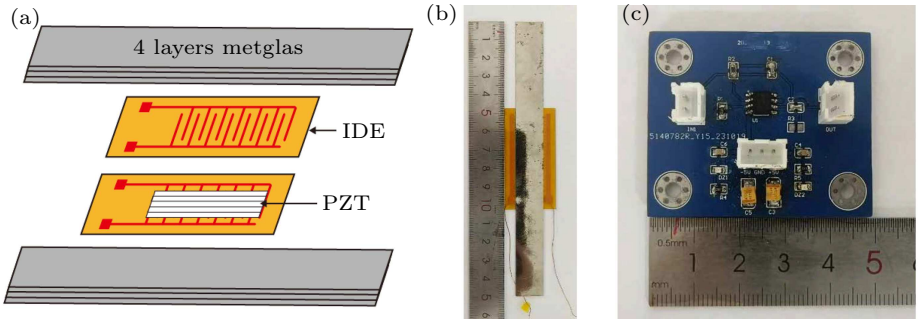


Fig. 3. (a) Structure diagram of ME sensing unit, (b) physical diagram of ME sensing unit, and (c) low-noise preamplifier.

The ME sensing unit consists mainly of a piezoelectric layer and a magnetostrictive layer. The piezoelectric layer is composed of five piezoelectric fibers $(\text{Pb}(\text{Zr}_x\text{Ti}_{1-x})\text{O}_3$, PZT TJ-60HD, Yunfu Ceramic Crystal Electronic Components Co., Ltd.) with dimensions of 40 mm (length) ×2 mm (width) ×0.2 mm (thickness) arranged in parallel. Two interdigital electrodes with a spacing of 850 μm were bonded to the upper and lower sides of the piezoelectric layer using epoxy resin

(West System 105 & 206), followed by polarization of the piezoelectric layer. Finally, four Metglas amorphous alloy ribbons with dimensions of 150 mm (length) ×15 mm (width) ×26 μm (thickness) were adhered to the upper and lower surfaces of the interdigital electrodes. The schematic diagram and physical diagram of the ME sensing unit are shown in Figs. 3(a) and 3(b). Since the direct electrical signal from the ME sensing unit is very weak and has high output impedance, a low-noise preamplifier circuit with high input impedance is typically connected to its output for signal amplification and impedance conversion, as shown in Fig. 3(c). The low-noise operational amplifier adopts AD795 of Analog Devices, with the feedback capacitance C_f of 100 pF and the parallel feedback resistance R_f of 200 MΩ. The detailed fabrication process of the ME sensing unit and the low-noise preamplifier can be referred to our previous work.[22,23]

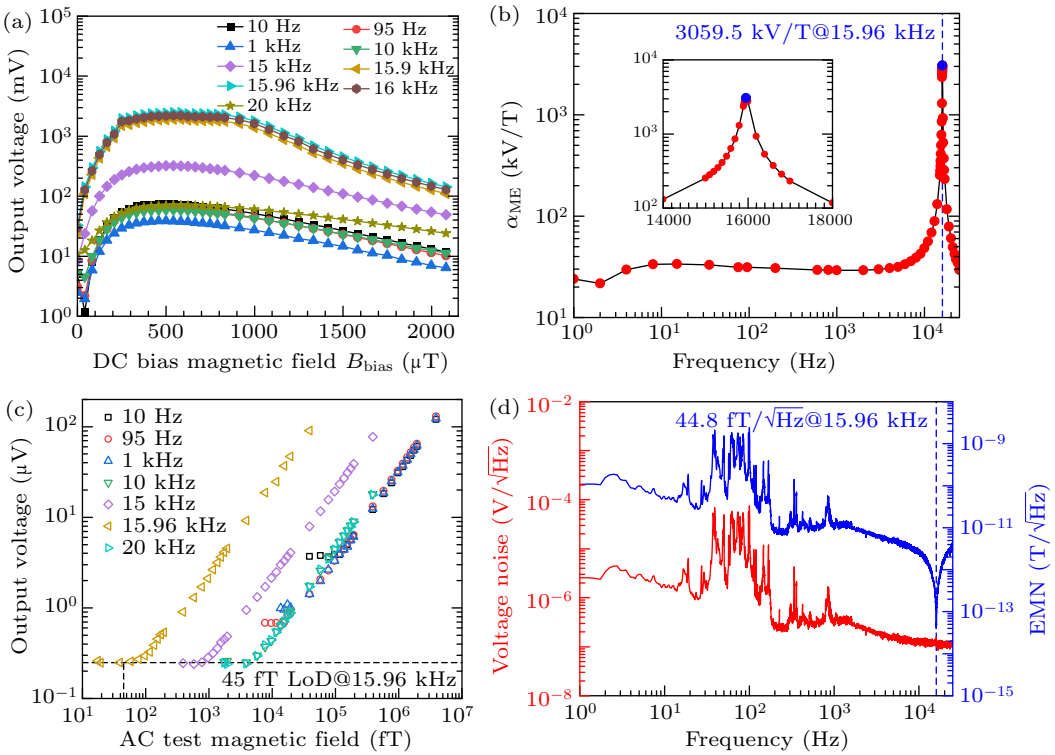


Fig. 4. The ME sensor (a) changes in response to AC test magnetic field under different DC bias magnetic fields, (b) magnetic field voltage coefficient, (c) output voltage varies with the frequency of the input magnetic field, (d) output voltage noise and equivalent magnetic field noise.

Next, the ME sensor was placed in a magnetically shielded room for performance testing. The signal with a frequency of 1 Hz to 25 kHz was generated by an AC current source (6221, Keithley, USA) into the Helmholtz coil $\text{Coil}_{\text{test}}$, which consists of a rectangular coil pair with a side length of 450 mm, the number of turns of 40, and a coil spacing of 200 mm. A DC bias magnetic field B_{bias} was applied through the coil with a diameter of 200 mm, 140 turns and a resistance of 11.3 Ω. The axes of the Helmholtz coil and the bias magnetic field coil were aligned, with the ME sensing unit positioned at the center of both coil axes, maintaining consistent alignment between the coil axis direction and the sensor's longitudinal direction. To determine the optimal bias field value of the ME sensing unit, firstly, the Helmholtz coil $\text{Coil}_{\text{test}}$ was made to generate an AC test magnetic field of 0.8 μT with frequencies gradually increasing from 10 Hz to 20 kHz. The bias magnetic field coil generated a DC bias magnetic field B_{bias} that gradually increased from 0 to 2080 μT. The output voltage signal of the ME sensor measured by an oscilloscope (DSO-X 4034A, Agilent, USA) is shown in Fig. 4(a). The voltage output of the ME sensor initially increases and then decreases with the increase of B_{bias}. When B_{bias} = 583 μT, the maximum output voltage of the ME sensor is 2.47 V at the frequency of 15.96 kHz, corresponding to the magnetic field voltage coefficient (α_{ME}) reaching the maximum value of 3088 kV/T. Due to the low magnetic field voltage coefficient under a zero-bias magnetic field, the ME sensing unit was positioned between two permanent magnets which can generate a 583-μT bias magnetic field to operate under the optimal bias magnetic field. Subsequently, the Helmholtz coil generated a 138-nT AC test magnetic field with frequency sweeping from 1 Hz to 25 kHz. The dynamic signal analyzer (35670A, Agilent, USA) was employed to measure the value of the output voltage signal of the preamplifier circuit, and the α_{ME} of the ME sensor in the range of 1 Hz–25 kHz is shown in Fig. 4(b), with an inset displaying α_{ME} near the resonant frequency. It

can be seen from the figure that the α_{ME} of the ME sensor reaches a peak value of 3059 kV/T at the resonant frequency of 15.96 kHz. Then the linear interval of the sensor was measured, with the frequency of the AC test magnetic field fixed at the resonant frequency of 15.96 kHz, and the magnetic field intensity gradually decreased from 40 pT to 20 fT. The output voltage of the ME sensor linearly decreased from 90 μV to 0.27 μV and then no longer decreased, and the limit of detection (LoD) of magnetic field intensity was 45 fT. The same method was used to test the minimum magnetic field detection limits of the ME sensor at different frequencies, and the results are shown in Fig. 4(c). Finally, the EMN of the ME sensor was measured in the absence of an excitation magnetic field signal, and the voltage noise of the ME sensor at 1 Hz–25 kHz was measured by the dynamic signal analyzer, as shown in the red curve in Fig. 4(d). The voltage noise divided by the α_{ME} yields the EMN of the ME sensor in a range of 1 Hz to 25 kHz. As shown in the blue curve in Fig. 4(d), the EMN of the sensor reaches 44.8 fT/$\sqrt{\text{Hz}}$ at the resonant frequency of 15.96 kHz, which is consistent with the minimum LoD of magnetic field at the resonant frequency.

3. Theoretical analysis

3.1. Working principle of the ME current sensor

The working principle of the ME current sensor is based on the magnetic effect of the current and the ME effect. Through the combination of these two effects, the measured current can be converted into the corresponding voltage signal. The current–magnetic field conversion coil converts the current I_{test} flowing through it into a magnetic field $B_{test} = \alpha_{coil} I_{test}$, where α_{coil} is the current–magnetic field conversion coefficient. The ME sensor converts the magnetic field B_{test} into a voltage $V_{test} = \alpha_{ME} I_{test}$, and α_{ME} is the magnetic field voltage coefficient. The sensitivity of the ME current sensor is the conversion coefficient $\alpha = \alpha_{ME}\alpha_{coil}$ between the input current I_{test} and the output voltage $V_{test} = \alpha I_{test}$. The radius r of the finite length solenoid Coil_{in} is 30 mm, the number of layers m is 2, the number of turns of each layer is n, the total number of turns is $N = nm$, the enameled copper wire diameter d is 0.5 mm, the coil length is $l = dn$, and μ_0 is the vacuum permeability. Assuming the input current is I_{test}, then for different coil turns n, the current–magnetic field conversion coefficient is[24]

$$\alpha_{coil} = \frac{B_{test}}{I_{test}} = \frac{\mu_0 nm}{\sqrt{4r^2 + l^2}} = \frac{\mu_0 nm}{\sqrt{4r^2 + (dn)^2}}. \tag{1}$$

From the above equation, when $dn \ll 2r$, $\alpha_{coil} = \mu nm/2r$, and α_{coil} increases linearly with the number of turns n of each layer of coils, when $2r$ is close to dn, α_{coil} slowly changes with the number of turns of the coil n, when $dn \gg 2r$, $\alpha_{coil} = \mu nm/dn = \mu m/d$, α_{coil} no longer changes with the number of turns of the coil n. The solid black line in Fig. 5 shows the relationship between the α_{coil} calculated by Eq. (1) and the n, and the α_{coil} increases linearly with the number of coil turns n, and finally remains almost constant. The black square, red dot, blue triangle, and green inverted triangle represent the α_{coil} of the coil (Coil I–Coil IV) with turns n of 10, 50, 200, and 400 turns obtained by Mag-13MSQ60 are 0.27 mT/A, 1.26 mT/A, 3.87 mT/A, and 5.44 mT/A, respectively, which are consistent with the theoretical calculation value. Therefore, if you want to increase the α_{coil} of the solenoid coil, you can reasonably increase the number of coil turns n.

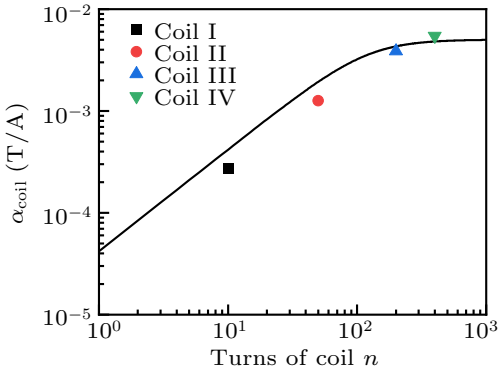


Fig. 5. The simulation and actual measurement of the solenoid coils' (Coils I–IV) current–magnetic field conversion coefficient.

3.2. Coupling and suppression of multisource noises

Figure 6 shows the multisource noise coupling mechanism of the ME current sensor. The internal resistance R of the solenoid coil Coil_{in} will introduce the current thermal noise I_{coil}, which is converted into magnetic field noise $B_{coil} = \alpha_{coil} I_{coil}$ through the solenoid coil. The magnetic field noise B_{coil} is coupled with the ambient magnetic field noise $B_{ambient}$ to the ME sensor, converted into output voltage noise. Meanwhile, the intrinsic magnetic field noise B_{ME} of the ME sensor is converted into output voltage noise, so the total output voltage noise is $V_{out} = \alpha_{ME}(B_{coil} + B_{ambient} + B_{ME})$. The ECN of the total output voltage noise of the ME current sensor is $I_{in} = V_{out}/\alpha = \alpha_{ME}(B_{coil} + B_{ambient} + B_{ME})/\alpha = I_{coil} + B_{ambient}/\alpha_{coil} + B_{ME}/\alpha_{coil}$. Thus, to reduce the ECN I_{in} of the current sensor, it is necessary to minimize the thermal current noise I_{coil} introduced by the internal resistance R of the solenoid coil, the ambient magnetic field noise $B_{ambient}$, and the intrinsic magnetic field noise B_{ME} of the ME sensor and increase the α_{coil} of the solenoid coil.

The intrinsic magnetic field noise B_{ME} of the ME sensor measured in Fig. 4(d), along with the current–magnetic field conversion coefficient α_{coil} measured in Fig. 5, can be used to calculate the ECN $I_{ME} = B_{ME}/\alpha_{coil}$, as shown by the solid line in Fig. 5.

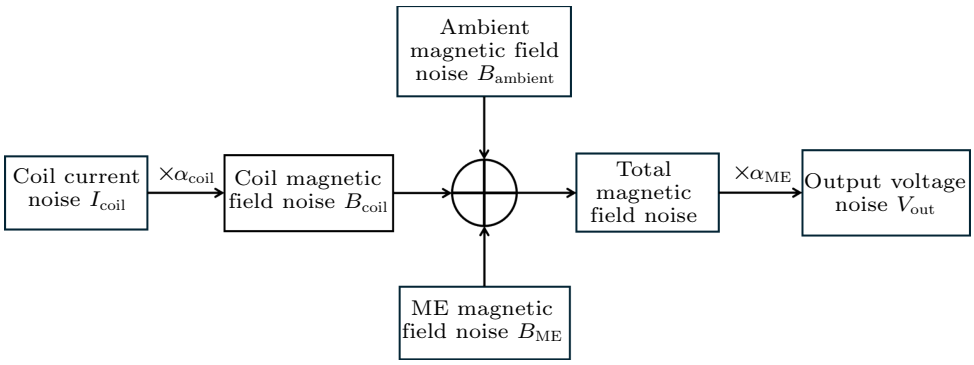


Fig. 6. Multisource noises coupling mechanism of the ME current sensor.

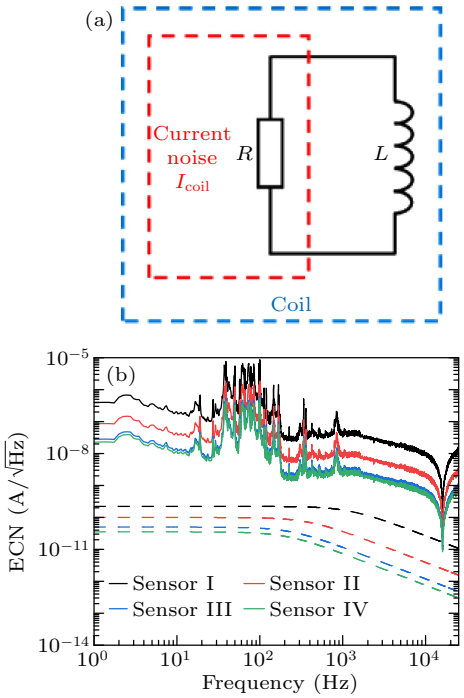


Fig. 7. (a) Equivalent model of current noise introduced by solenoid coil. (b) The solid line represents the ECN I_{ME} of the ME current sensor is obtained by dividing the magnetic field noise B_{ME} by the current–magnetic field conversion coefficient α_{coil} of the coil, and the dashed line represents the simulation result of the current noise I_{coil} introduced by the internal resistance R of the coil.

The solenoid coil Coil_{in} internal resistance R will introduce current thermal noise I_{coil}[25]

$$I_{coil} = \sqrt{\frac{4kTR}{R^2+\omega^2L^2}} = \sqrt{\frac{4kTN\rho}{(N\rho)^2+(2\pi fL)^2}}. \tag{2}$$

Among them, ρ is the resistance value of one turn of the coil, k is the Boltzmann constant, T is the room temperature 300 K, L is the inductance of a solenoid coil, and its calculation method[26]

$$L = \frac{\mu_0\pi r^2N^2}{l+0.9004r}, \tag{3}$$

where r is the radius of the finite length solenoid, N is the total number of turns, and l is the coil length. From the above formula, we can numerically calculate the relationship between the internal resistance R of the solenoid coil introducing the current thermal noise I_{coil} with frequency, as shown in the dashed line in Fig. 7(b).

Without considering the ambient magnetic field noise $B_{ambient}$, as shown in Fig. 7(b), for these four solenoid coils, the thermal noise I_{coil} of the internal resistance R introduced by the solenoid coils Coil_{in} is much smaller than the ECN I_{ME} introduced by the intrinsic magnetic field noise B_{ME} of the ME sensor, $I_{coil} \ll I_{ME} = B_{ME}/\alpha_{coil}$. Therefore, to obtain a low-noise current sensor, the α_{coil} of the solenoid coil should be increased as much as possible, such as reasonably increasing the number of coil turns, decreasing the coil radius, and other parameters, so as to effectively reduce the ECN of the current sensor. Here, the solenoid coil Coil IV, with 2 layers and 400 turns of a single-layer coil, has the α_{coil} of 5.44 mT/A and is used in a low-noise ME current sensor.

4. Results and discussion

The performance of the ME current sensor IV, comprising the solenoid coil IV with a total of 800 turns and an ME sensor, was systematically evaluated. An AC current source was used to apply a current signal of 15.96 kHz (the resonant frequency of the ME sensor) to the solenoid coil, and the values of the current signals were set sequentially to 10 nA_{pp}, 20 nA_{pp}, 30 nA_{pp}, and 40 nA_{pp}. Despite interference from other frequency signals, the voltage signal waveform of the ME current sensor IV after undergoing 10^4-voltage amplification still allowed the observation of corresponding voltage signal waveforms on the oscilloscope, as illustrated in Fig. 8.

The frequency of the test current I_{test} applied by the AC current source was fixed at the resonant frequency of 15.96 kHz, which was gradually reduced from 40 nA_{pp}. The spectrum information of the output voltage V_{test} of the ME current sensor IV was recorded by the dynamic signal analyzer. A 15.96 kHz current signal as low as 60 pA_{pp} (21.21 pA_{rms}) can be clearly observed, as shown by the blue curve in Fig. 9. The relationship between the value of the test current I_{test} and the value of the output voltage V_{test} of the ME current sensor IV is shown in Fig. 10. With the decrease of the test current at the resonant frequency, the output voltage of the ME current sensor linearly decreases to about 270 nV and then no longer decreases; at this time, the LoD of the test current signal is about 10 pA_{rms}.

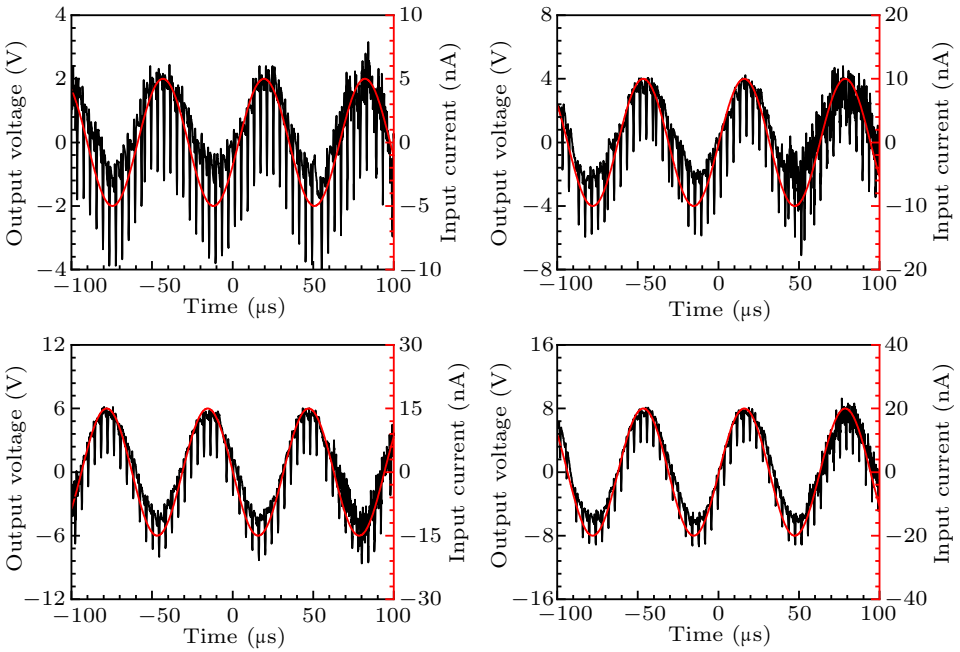


Fig. 8. When the input with currents of 10 nA_{pp} , 20 nA_{pp}, 30 nA_{pp}, and 40 nA_{pp} at a frequency of 15.96 kHz, the output voltages of the ME current sensor IV undergoing 10^4-voltage amplification are obtained.

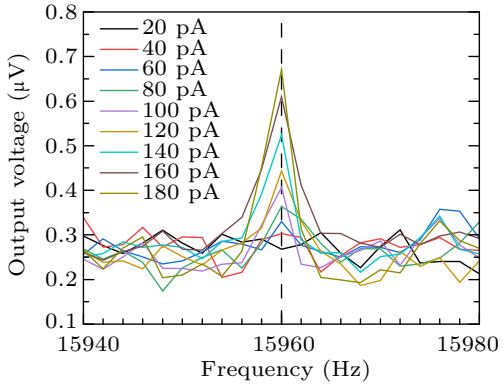


Fig. 9. The output voltage of the ME current sensor IV is observed under the dynamic signal analyzer when the value of the input current drops from 180 pA_{pp} to 20 pA_{pp} at a frequency of 15.96 kHz.

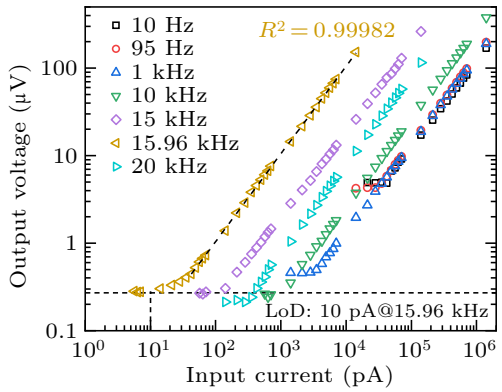


Fig. 10. The linear variation of the output voltage and input current of the ME current sensor IV at different frequencies and their limit of detection are measured by the dynamic signal analyzer.

The slope of the linear relationship between the output voltage V_{test} and the test current I_{test} is shown in Fig. 10, which is the current–voltage conversion coefficient α of the ME current sensor IV. It can be concluded that its linearity R^2 reaches 0.99982. By varying the frequency of the test current, the frequency response curve of the ME current sensor IV conversion coefficient α with frequency can be measured, as shown in Fig. 11(a). Notably, the current–voltage conversion coefficient of the ME current sensor IV is 17.36 V/mA at the resonant frequency of 15.96 kHz. In the absence of an excitation current signal, the ME current sensor was placed in the magnetic shielded room, and the voltage noise of the ME current sensor IV at 1 Hz–25 kHz was

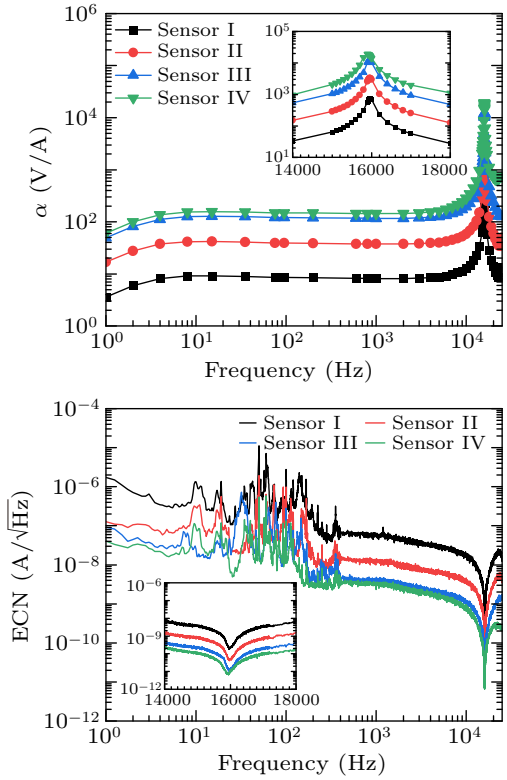


Fig. 11. ME current sensors I–IV at 1 Hz–25 kHz (a) current–voltage conversion coefficient and (b) equivalent current noise.

measured by the dynamic signal analyzer. The voltage noise is divided by the current–voltage conversion coefficient α to obtain the ECN, as shown by the green curve in Fig. 11(b). The ECN in th frequency range of 400 Hz–25 kHz is no higher than 10 nA/$\sqrt{\text{Hz}}$, and the ECN in the frequency range of 1 Hz–400 Hz is no higher than 600 nA/$\sqrt{\text{Hz}}$. In addition, the illustration in Fig. 11(b) shows the ECN of the sensor at 14 kHz–18 kHz, the ECN of the ME current sensor IV reaches 8.4 pA/$\sqrt{\text{Hz}}$ at the resonant frequency, which is basically consistent with its minimum current detection limit. Similarly, the ECN at the resonant frequency of the ME current sensors I, II, and III, which compose of solenoid coils with total turns N of 20, 100, and 400 and ME sensors is 197 pA/$\sqrt{\text{Hz}}$, 46 pA/$\sqrt{\text{Hz}}$, and 12.3 pA/$\sqrt{\text{Hz}}$ respectively, as shown by the black, red and blue curves in Fig. 11(b).

To evaluate the environmental interference immunity of the ME current sensor, the noise levels of the current sensor IV inside and outside the shielded room were compared, as shown in Fig. 12. Although the ME current sensor IV is interfered with by the external magnetic field outside the shielded room, the interference is basically concentrated below 1 kHz, and the ECN at its resonant frequency can still reach 11.5 pA/$\sqrt{\text{Hz}}$. Table 1 shows the comparison with other current magnetic field sensors. Although the performance is average at low frequencies, the ME current sensor in this paper at the resonant frequency is similar to that of the SQUID current sensor, reaching the pA level, which is four orders of magnitude lower than traditional ME current sensors.

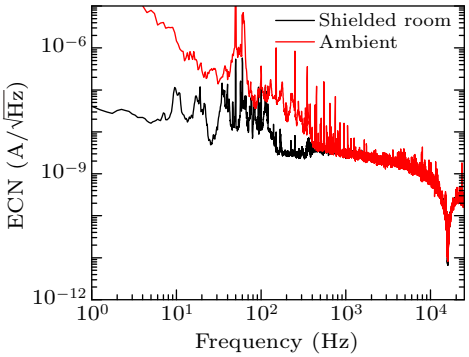


Fig. 12. The ECN measured inside and outside the shielded room using the ME current sensor IV.

Table 1. Performance comparison of different current sensors.

Ref.	Sensors	Current noise			
		1 Hz	10 Hz	1 kHz	Other frequency
[11]	coil_{in} + SQUID	NA	1 pA/$\sqrt{\text{Hz}}$	1 pA/$\sqrt{\text{Hz}}$	1–2 pA/$\sqrt{\text{Hz}}$@5 Hz∼10 kHz
[12]	coil_{in} + SQUID	7 pA/$\sqrt{\text{Hz}}$	3 pA/$\sqrt{\text{Hz}}$	1.5 pA/$\sqrt{\text{Hz}}$	1–100 pA/$\sqrt{\text{Hz}}$@0.2 Hz∼51.2 kHz
[13]	coil_{in} + SQUID	3.8 pA/$\sqrt{\text{Hz}}$	4.2 pA/$\sqrt{\text{Hz}}$	1.6 pA/$\sqrt{\text{Hz}}$	0.5–4.2 pA/$\sqrt{\text{Hz}}$@1 Hz∼1 kHz
	coil_{in} with transformers + SQUID	18 fA/$\sqrt{\text{Hz}}$	20 fA/$\sqrt{\text{Hz}}$	8 fA/$\sqrt{\text{Hz}}$	2.3–20 fA/$\sqrt{\text{Hz}}$@1 Hz∼1 kHz
[15]	magnetic core + Hall	0.4 mA/$\sqrt{\text{Hz}}$	0.3 mA/$\sqrt{\text{Hz}}$	0.3 mA/$\sqrt{\text{Hz}}$	30 μA/$\sqrt{\text{Hz}}$@1 MHz
[16]	magnetic core + TMR	70 μA/$\sqrt{\text{Hz}}$	20 μA/$\sqrt{\text{Hz}}$	4 μA/$\sqrt{\text{Hz}}$	2.5 μA/$\sqrt{\text{Hz}}$@2.5 kHz
[17]	magnetic core + Fluxgate	NA	NA	NA	200 μA/$\sqrt{\text{Hz}}$@50 Hz
[19]	coil_{in} + ME	920 nA/$\sqrt{\text{Hz}}$	NA	NA	94 nA/$\sqrt{\text{Hz}}$@f_{r}
[20]	coil_{in} + ME	NA	NA	NA	15 mA/$\sqrt{\text{Hz}}$@f_{r}
[21]	coil_{in} + ME	20 mA/$\sqrt{\text{Hz}}$	0.5 mA/$\sqrt{\text{Hz}}$	30 μA/$\sqrt{\text{Hz}}$	0.6 μA/$\sqrt{\text{Hz}}$@f_{r}
[27]	magnetic core + ME	NA	NA	NA	0.43 μA/$\sqrt{\text{Hz}}$@f_{r}
This work	coil_{in} + ME	40 nA/$\sqrt{\text{Hz}}$	87 nA/$\sqrt{\text{Hz}}$	3 nA/$\sqrt{\text{Hz}}$	8.4 pA/$\sqrt{\text{Hz}}$@f_{r}

f_{r}: the resonance frequency of the ME sensor.

5. Conclusion

We have developed an ME current sensor comprising a current–magnetic field conversion coil and an ME sensing unit integrated with a low-noise preamplifier, enabling indirect current–voltage conversion. The coupling mechanisms of current noise were thoroughly analyzed to optimize the system's performance. The current ME sensor was systematically characterized, achieving the ECN of 8.4 pA/$\sqrt{\text{Hz}}$ at its resonant frequency of 15.96 kHz, with the ECN values below 10 nA/$\sqrt{\text{Hz}}$ in the 400 Hz–25 kHz frequency range and below 600 nA/$\sqrt{\text{Hz}}$ in the frequency range of 1 Hz–400 Hz. Finally, if the ME conversion coefficient of the ME sensing unit is further increased by increasing the number of layers of Metglas, or a transformer is added at the input end, it is completely possible to achieve the measurement of weak current signals of several hundred fA levels at the resonant frequency.

References

[1] Yi Z X, Chen Z L, Yin K, Wang L C and Wang K 2023 *Prot. Control Mod. Power Syst.* **8** 1
[2] Friedrich N, Rosławska A, Arrieta X, Kaiser K, Romeo M, Le Moal E, Scheurer F, Aizpurua J, Borisov A G, Neuman T and Schull G 2024 *Nat. Commun.* **15** 9733
[3] Nandan K, Keshari N, Naseer A, Agarwal A, Bhowmick S and Chauhan Y S 2025 *IEEE Trans. Electron Dev.* **72** 516
[4] Abbasi R, Ackermann M, Adams J, Agarwalla S K, Aguilar J A, Ahlers M, Alameddine J M, Amin N M and Andeen K 2024 *Phys. Rev. D* **110** 022001
[5] Huang Y H, Zhou M H, Yu A D, Peng S and Xia L 2022 *Opt. Laser Technol.* **151** 107995
[6] Nakashima Y, Hirayama F, Kohjiro S, Yamamori H, Nagasawa S, Sato A, Yamasaki N Y and Mitsuda K 2019 *IEEE Trans. Appl. Supercond.* **29** 2100705

[7] Gramolin A V, Aybas D, Johnson D, Adam J and Sushkov A O 2021 *Nat. Phys.* **17** 79
[8] Ullom J N and Bennett D A 2015 *Supercond. Sci. Technol.* **28** 084003
[9] Henderson S W, Ahmed Z, Austermann J, Becker D, Bennett D A, Brown D, Chaudhuri S, Cho H S, D'Ewart J M, Dober B, Duff S M, Dusatko J E, Fatigoni S, Frisch J C, Gard J D, Halpern M, Hilton G C, Hubmayr J, Irwin K D, Karpel E D, Kernasovskiy S S, Kuenstner S E, Kuo C L, Li D, Mates J A B, Reintsema C D, Smith S R, Ullom J, Vale L R, Van Winkle D D, Vissers M and Yu C 2018 *Millimeter, Submillimeter, and Far-Infrared Detectors and Instrumentation for Astronomy IX*, 2018, Austin, Texas, USA, p. 284
[10] Xu D, Li J J, Wang S J, Ma M Z, Cao W H, Wang X S, Zhang M Y, Zhao J T and Zhong Q 2022 *Supercond. Sci. Technol.* **35** 085004
[11] Vettoliere A and Granata C 2022 *Appl. Sci.* **12** 9030
[12] Ni Z, Zhang G F, Wu J, Qiu L Q, Liu X Y, Dong H, Rong L L and Xie X M 2024 *IEEE Trans. Appl. Supercond.* **34** 1100704
[13] Kleinbaum E, Shingla V and Csáthy G A 2017 *Rev. Sci. Instrum.* **88** 034902
[14] Schmelz M, Shvab V, Peiselt K, Kunert J, Zakosarenko V, Stöhlker T, Oelsner G and Stolz R 2025 *IEEE Trans. Appl. Supercond.* **35** 0600704
[15] Crescentini M, Marchesi M, Romani A, Tartagni M and Traverso P A 2018 *IEEE Trans. Instrum. Meas.* **67** 1470
[16] Liu J M, Guan M M, Xu Y W, Zhao S, Su W, Zhang C L, Wang Z G, Zhang X H, Hu Z Q, Jiang Z D and Liu M 2023 *IEEE Trans. Instrum. Meas.* **72** 2008009
[17] Snoeij M F, Schaffer V, Udayashankar S and Ivanov M V 2016 *IEEE J. Solid-State Circuits* **51** 1684
[18] Luo B, Will-Cole A R, Dong C Z, He Y F, Liu X X, Lin H, Huang R, Shi X L, McConney M, Page M, Sanghadasa M, Ramesh R and Sun N X 2024 *Nature Reviews Electrical Engineering* **1** 317
[19] Dong S X, Bai J G, Zhai J Y, Li J F, Lu G Q, Viehland D, Zhang S J and Shrout T R 2005 *Appl. Phys. Lett.* **86** 182506
[20] Yu X J, Lou G F, Chen H, Wen C and Lu S H 2015 *IEEE Sens. J.* **15** 5839
[21] Zhang M J and Or S W 2018 *Sensors* **18** 588
[22] Zhou H M, Chen J J, Fang Y Q, Xu Z T, Chang K, Yu G L, Zhu M M and Qiu Y 2023 *IEEE Sens. J.* **23** 13019
[23] Xiao Y, Zhou H M and Gou X F 2018 *Comput. Mater. Contin.* **54** 209
[24] Martín-Luna P, Gimeno B, González-Iglesias D, Esperante D, Blanch C, Fuster-Martínez N, Martinez-Reviriego P and Fuster J 2023 *IEEE Trans. Magn.* **59** 7000106
[25] Lusher C P, Li J, Maidanov V A, Digby M E, Dyball H, Casey A, Nyéki J, Dmitriev V V, Cowan B P and Saunders J 2001 *Meas. Sci. Technol.* **12** 1
[26] Yeon P, Rajan S K, Falcone J, Gonzalez J L, May G S, Bellamkonda R V, Brand O, Bakir M S and Ghovanloo M 2021 *IEEE Sens. J.* **21** 13837
[27] Qiao J C, Wu J G, Fan F Z, Liang X F, Wang G Y, Du Y J, Xu Y W, Zhang M, Hu Z Q and Liu M 2025 *IEEE Trans. Instrum. Meas.* **74** 9001411